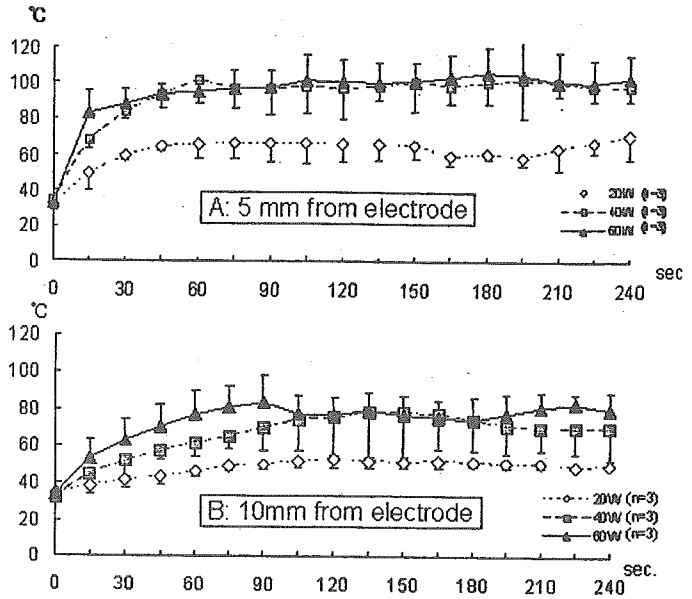

FIG. 3. (A) At 5 mm from the electrode, the temperature rose rapidly to 85°C (for 15 s at 60 W and 30 s at 40 W). The temperature reached a plateau around 90-100°C at 40 and 60 W. There was no significant difference between 40 and 60 W for each time point. (B) At 10 mm from the electrode, the temperature rose gradually to 70°C (45 s at 60 W and 90 s at 40 W). The temperature reached a plateau around 80°C at 40 and 60 W. There was no significant difference between 40 and 60 W for each time point.

sponse was obtained in the two groups of 40 W and 60 W at same distances from the electrode.

Measurements of Coagulation Area

The data of the diameter of the maximum coagulation area in the animal model is shown in Fig. 4. The maximum coagulation area increased with increased power and coagulation time. The diameter of the maximum coagulation area was 18.3 ± 10.4 mm at 40 W for 4 min and 21.7 ± 2.9 mm at 60 W for 4 min. There was no significant difference in the coagulation area at each time period when using 40 W and 60 W.

The diameter of the maximum coagulation area in normal human fresh lung tissue after resection of central-type lung cancer is shown in Fig. 5. The maximum coagulation area increased with increased power and coagulation time until 3 min. After 3 min, the diameter of the maximum coagulation area was 25 mm at 40 W and 26 mm at 60 W. At 40 and 60 W for 4 min, the diameter of the maximum coagulation area shrank to 15 mm. There was no difference between 40 and 60 W for each period of coagulation.

Histological Examinations after Microwave Coagulation

All beagles tolerated the procedure well. During 6 months of follow up to assess histological change of the coagulated tissue, the normal activity and condition of each beagle was monitored daily. There was no death due to serious complications such as hemoptysis or pneumothorax during the period.

The histological changes after microwave coagulation are shown in Fig. 6. Histological findings shortly after microwave coagulation showed degeneration and thickening of collagen fiber and exfoliation and ulceration of bronchial epithelium surrounding the electrode. No surrounding bronchioli or veins were destroyed. No blood clots or debris were observed in surrounding veins (Fig. 6A). After 3 months, histological findings showed stromal edema and loose collagen fiber, immature neoangiogenesis, progression of bronchial epithelial hyperplasia, infiltration of inflammatory cells at the boundary zone (lymphocyte > plasma cell > neutrophil) between the central coagulation area and normal tissue (Fig. 6B). After 6 months, coagulated tissue became scar tissue that showed disappearance of stromal edema, tight collagen fiber, mature capillaries, disappearance of inflammatory cells, and completion of epithelial hyperplasia (Fig. 6C).

DISCUSSION

With the increasing use of high-resolution CT scans, the rate detection of small nodules in the peripheral lung, such as early-stage lung cancer, small metastases, or AAH has increased. Kaneko *et al.* demonstrated that the detection rate of peripheral lung carcinoma by mass screening using CT scan was 0.45% (15 of 3457 examinations), 73% of which were detected by low-dose spiral CT but were not visible on standard chest radiography [5]. Noguchi *et al.* investigated 236 surgically resected small-size peripheral adenocarcinomas measuring 2.0 cm or less in greatest dimension and demonstrated that type A (localized bronchioloalveolar carcinoma: LBAC) and type B (LBAC with foci of structural collapse of alveoli) that showed ground glass opacity (GGO) on CT scanning images demonstrated

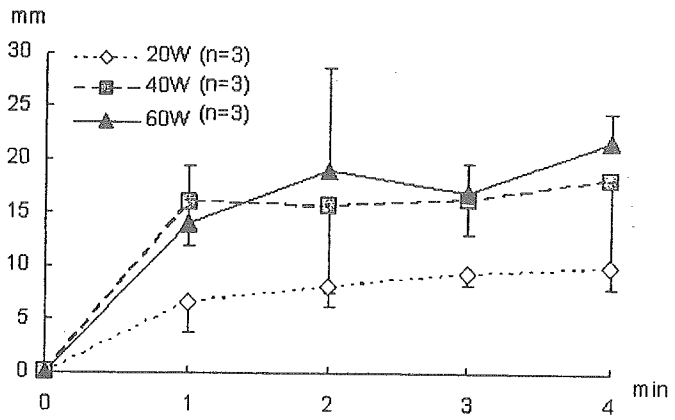

FIG. 4. The diameter of the maximum coagulation area was 18 mm at 40 W for 4 min and 22 mm at 60 W for 4 min. There was no significant difference between 40 W and 60 W for each coagulation time.

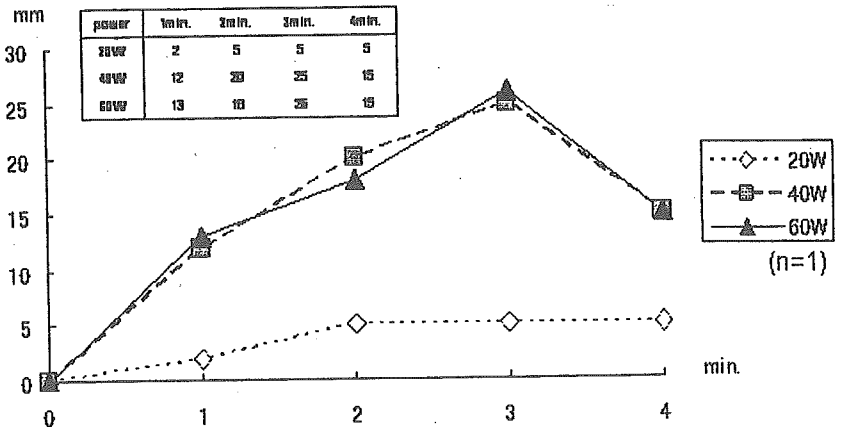

FIG. 5. The diameter of the maximum coagulation area was 25 mm at 40 W and 60 W for 3 min. There was no difference between 40 and 60 W for each time. The diameter of the maximum coagulation area shrank to 15 mm at 40 and 60 W for 4 min.

no lymph node metastasis and had the best 5-year survival rate (100%) [6]. Meanwhile, according to a pathological study on lymph node metastasis of primary lung carcinoma after surgery, the rate of metastasis (N1 and N2) was 0% with a tumor 1.0 cm or less, 17% with a tumor 1.1 to 2.0 cm, and 37% with a tumor 2.1 to 3.0 cm in diameter [7]. As a result, it seems to be possible to control 83% of lung carcinomas smaller than 2.0 cm in size by local treatment. Also, the rate of local lymph node metastasis of metastatic lung tumor is known to be low.

We usually perform surgery for such patients as a possible cure, but this may lead to considerable lung damage with significant loss of function. Although VATS has widened the indication of surgery recently, some patients are unable to undergo even VATS due to poor cardiopulmonary function, severe adhesion, or advanced age, etc. Radical radiotherapy or chemotherapy or both may be offered with curative intent to such patients, but the prospect of cure is substantially worse than with surgical options, while it may also lead to considerable lung damage with significant loss of function caused by radiation fibrosis, systemic toxicity due to the anticancer agent. Therefore, new modalities for local treatment that effectively destroy tumor but are less invasive and less damaging to normal lung tissue are required. Recently, several investigators tried to use radiofrequency ablation (RFA) [8–10] or photodynamic therapy (PDT) for peripheral lung tumors [11, 12].

We are interested in microwave coagulation therapy (MCT), which has been successfully used to perform coagulation of hepatic tumors. In 1978, hepatic surgery with MCT was introduced by Tabuse [1], and recently the effectiveness of percutaneous microwave coagulation therapy (PMCT) under ultrasonography or CT scan guidance for small hepatocellular carcinoma was demonstrated [3, 4]. We considered this modality to be applicable for patients with lung tumors who are poor surgical candidates, as well as patients with hepatic tumors, and evaluated the efficacy and safety of MCT for lung tissue experimentally.

The microwave generator emits a higher frequency wavelength than electrocautery and generates dielectric heat energy due to friction of water molecules when irradiating living tissue. MCT applies this mechanism to achieve tumor necrosis. Because the dielectric heat energy cannot be generated in the presence of air, selective tumor damage may be achieved, with limited damage to the surrounding normal air-filled lung tissue. We considered it essential to know how MCT affects normal lung tissue before performing PMCT clinically for peripheral lung malignancies. An experimental study was deemed necessary to evaluate the thermal response, coagulation extent, and histological changes in the air-filled normal lung.

With regard to thermal response, the temperatures of normal canine lung tissue rose with increased microwave power and coagulation time. The temperatures in normal lung tissue rose to 90-100°C at 5 mm from the electrode after 60 s and 70-80°C at 10 mm after 90 s, thereafter reaching a plateau. A power of 20 W was not sufficient to coagulate lung tissue. These data suggested that the same thermal response could be obtained at 40 and 60 W. The coagulation area in normal canine lung tissue increased to 18 mm and 22 mm at 40 W and 60 W for 4 min, respectively. Therefore, it may be possible to coagulate a diameter of approximately 20 mm. In solid tumors, there is a possibility to achieve more extensive coagulation. In human resected normal lung with central-type lung carcinoma, the coagulation area increased to 25 mm at 40 and 60 W for 3 min and shrank to 15 mm for 4 min. This phenomenon may be explained by shrinking of lung tissue due to rapid elevation of the temperature in the tissue, because there is no radiator effect in the resected lung due to the lack of blood supply. From the current study, we concluded the optimal condition in clinical PMCT to be 40-60 W for 3–4 min of coagulation.

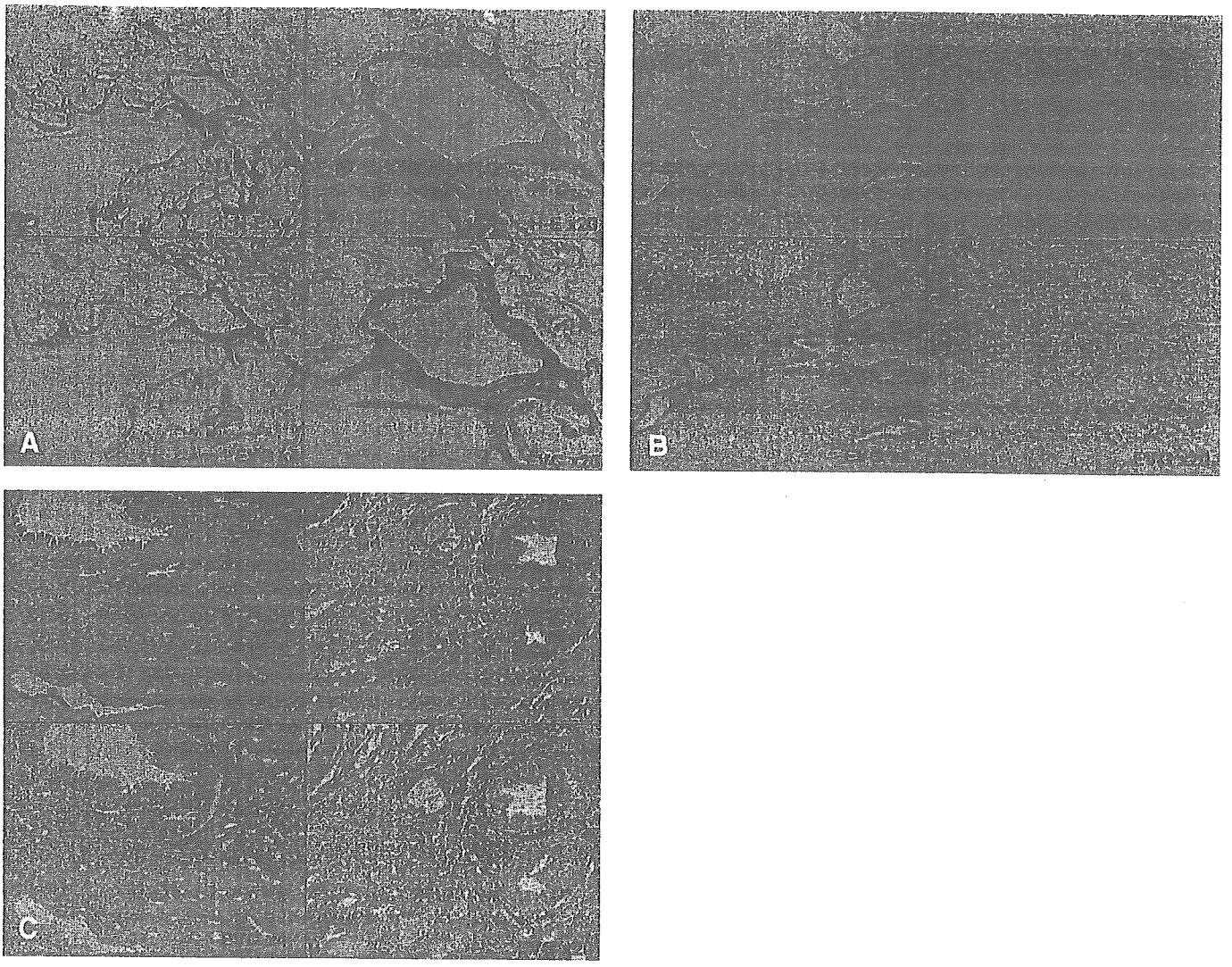

FIG. 6. (A) Histological findings shortly after microwave coagulation showed degeneration and thickening of collagen fiber and exfoliation and ulceration of bronchial epithelium surrounding the electrode. Surrounding bronchial and veins were not destroyed. (B) After 3 months, histological findings showed stromal edema and loose collagen fiber, immature neoangiogenesis, progression of bronchiolus epithelial hyperplasia, infiltration of inflammatory cells at the boundary zone between the central coagulation area and normal tissue. (C) After 6 months, coagulated tissue became scar tissue that showed disappearance of stromal edema, tight collagen fiber, mature capillaries, disappearance of inflammatory cells and completion of epithelial hyperplasia. (Color version of figure is available online.)

Histological analysis following MCT for normal canine lung tissue demonstrated exfoliation and ulcer formation of the epithelium in the bronchioli and degeneration and thickening of collagen fiber in the parenchyma by heat coagulation shortly after MCT. The coagulated lesions were gradually repaired by progression of epithelial hyperplasia and infiltration of inflammatory cells, showing stromal edema and granulation tissue after 3 months and finally becoming scar tissue after 6 months. We concluded MCT to be a safe modality for lung tissue because no destruction of bronchioles or veins was seen in the specimens during 6 months.

The present studies of MCT for peripheral lung tissue demonstrated that this new modality had no serious adverse effects and could be performed safely. However, the incidence of pneumothorax by CT-guided RFA was demonstrated to be 38.5% (3/8) in a rabbit model [8] and 33.3% (1/3) and 53.8% (7/13) in clinical cases [9, 10], which seems to be relatively high. Therefore, the development of a fine electrode with a cooling system will be necessary to prevent complications such as pneumothorax and heat sensation for clinical use.

From our experimental studies, the advantages of PMCT are the fact that this modality is minimally invasive, may be performed by local anesthesia, and is applicable for patients with poor cardiopulmonary function. In addition, the microwave generator is a very simple device, maintenance free, easy to handle, and portable, and the procedure is easy compared with RFA and PDT. The possibility of pneumothorax, heat

sensation or pain, or both during treatment and the limited coagulation area are considered the disadvantages for clinical use at present. Nevertheless, our results demonstrated the possibility of MCT for patients with small peripheral lung tumors with the intent of curative treatment. Although MCT is considered to be a useful modality as minimally invasive therapy for small peripheral lung tumors, further comparative research is necessary with other modalities such as RFA and PDT for peripheral lung tumors.

REFERENCES

1. Tabuse, K. A new operative procedure of hepatic surgery using a microwave tissue coagulation. *Arch. Jpn. Chir.* **48:** 160, 1979.
2. Hamazoe, R., Hirooka, Y., Ohtani, S., *et al.* Intraoperative microwave tissue coagulation as treatment for patients with nonresectable hepatocellular carcinoma. *Cancer* **75:** 794, 1995.
3. Seki, T., Wakabayashi, M., Nakagawa, T., *et al.* Ultrasonically guided percutaneous microwave coagulation therapy for small hepatocellular carcinoma. *Cancer* **74:** 817, 1994.
4. Ohmoto, K., Miyake, I., Tsuduki, M., *et al.* Percutaneous microwave coagulation therapy for unresectable hepatocellular carcinoma. *Hepatogastroenterology* **46:** 2894, 1999.
5. Kaneko, M., Eguchi, K., Ohmatsu, H., *et al.* Peripheral lung cancer: screening and detection with low-dose spiral CT versus radiography. *Radiology* **201:** 798, 1996.
6. Noguchi, M., Morikawa, A., Kawasaki, M., *et al.* Small adenocarcinoma of the lung. Histologic characteristics and prognosis. *Cancer* **75:** 2844, 1995.
7. Ishida, T., Yano, T., Maeda, K., *et al.* Strategy for lymphadenopathy in lung cancer three cm or less in diameter. *Ann. Thorac. Surg.* **50:** 708, 1990.
8. Goldberg, S. N., Gazelle, G. S., Compton, C. C., *et al.* Radiofrequency tissue ablation in the rabbit lung: efficacy and complications. *Acad. Radiol.* **2:** 776, 1995.
9. Dupuy, D. E., Zagoria, R. J., Akerley, W., *et al.* Percutaneous radiofrequency ablation of malignancies in the lung. *AJR Am. J. Roentgenol.* **174:** 57, 2000.
10. Herrera, L. J., Fernando, H. C., Perry, Y., *et al.* Radiofrequency ablation of pulmonary malignant tumors in nonsurgical candidates. *J. Thorac. Cardiovasc. Surg.* **125:** 929, 2003.
11. Fielding, D. I., Buonaccorsi, G. A., MacRobert, A. J., *et al.* Fine-needle interstitial photodynamic therapy of the lung parenchyma. *Chest* **155:** 502, 1999.
12. Okunaka, T., Kato, H., Tsutsui, H., *et al.* Photodynamic therapy for peripheral lung cancer. *Lung Cancer* **43:** 77, 2004.

ELSEVIER

Int. J. Radiation Oncology Biol. Phys., Vol. 61, No. 4, pp. 1117–1122, 2005

0360-3016/05/$–see front matter

doi:10.1016/j.ijrobp.2004.07.692

CLINICAL INVESTIGATION — Lung

A PHASE II STUDY OF HYPERFRACTIONATED ACCELERATED RADIOTHERAPY (HART) AFTER INDUCTION CISPLATIN (CDDP) AND VINORELBINE (VNR) FOR STAGE III NON-SMALL-CELL LUNG CANCER (NSCLC)

SATOSHI ISHIKURA, M.D.,* YUICHIRO OHE, M.D.,† KEIJI NIHEI, M.D.,* KAORU KUBOTA, M.D.,† RYUTARO KAKINUMA, M.D.,† HIRONOBU OHMATSU, M.D.,† KOICHI GOTO, M.D.,† SEIJI NIHO, M.D.,† YUTAKA NISHIWAKI, M.D.,† AND TAKASHI OGINO, M.D.*

*Divisions of Radiation Oncology and †Thoracic Oncology, National Cancer Center Hospital East, Kashiwa, Chiba, Japan

Purpose: The purpose was to assess the feasibility and efficacy of hyperfractionated accelerated radiotherapy (HART) after induction chemotherapy for Stage III non-small-cell lung cancer.

Methods and Materials: Treatment consisted of 2 cycles of cisplatin 80 mg/m^2 on Day 1 and vinorelbine 25 mg/m^2 on Days 1 and 8 every 3 weeks followed by HART, 3 times a day (1.5, 1.8, 1.5 Gy, 4-h interval) for a total dose of 57.6 Gy.

Results: Thirty patients were eligible. Their median age was 64 years (range, 46–73 years), 24 were male, 6 were female, 8 had performance status (PS) 0, 22 had PS 1, 9 had Stage IIIA, and 21 had Stage IIIB. All but 1 patient completed the treatment. Common grade ≥3 toxicities during the treatment included neutropenia, 25; infection, 5; esophagitis, 5; and radiation pneumonitis, 3. The overall response rate was 83%. The median survival was 24 months (95% confidence interval [CI], 13–34 months), and the 2-year overall survival was 50% (95% CI, 32–68%). The median progression-free survival was 10 months (95% CI, 8–20 months).

Conclusion: Hyperfractionated accelerated radiotherapy after induction of cisplatin and vinorelbine was feasible and promising. Future investigation employing dose-intensified radiotherapy in combination with chemotherapy is needed.

Non-small-cell lung cancer, Hyperfractionated accelerated radiation therapy, Chemoradiotherapy.

INTRODUCTION

Lung cancer is the leading cause of cancer-related death for men and the second for women in Japan. During 2001, approximately 55,000 patients died of lung and bronchus cancer (1). Surgery is the standard of care for patients with Stage I–II non–small-cell lung cancer (NSCLC), but a combination of chemotherapy and thoracic radiotherapy with or without surgery is indicated for the majority of patients with Stage III disease. Cisplatin (CDDP) based chemotherapy with conventional radiotherapy improved survival compared to conventional radiotherapy alone (2–6) and was the standard of care in the 1990s. Recently, concurrent chemoradiotherapy has been revealed to be superior to sequential chemoradiotherapy (7, 8), but it is difficult to give full-dose chemotherapy using newer cytotoxic agents concurrently with radiotherapy, and the optimal combination has not yet been clarified. In the meantime, continuous hyperfractionated accelerated radiotherapy (CHART) with 3 daily fractions to intensify the local effect of radiotherapy has been found to be superior to conventional radiotherapy (9). The survival benefit of CHART was encouraging, but the protocol including treatments on weekends and 6-h intervals between fractions had some difficulties in practicality. Mehta *et al.* introduced hyperfractionated accelerated radiotherapy (HART) (modified CHART) with 3 daily fractions and 4-h interfraction intervals with weekend breaks and also showed promising results similar to those using sequential chemoradiotherapy (10). After these results, we started a Phase II trial to evaluate the feasibility and efficacy of induction chemotherapy with HART for patients with Stage III NSCLC.

METHODS AND MATERIALS

Eligibility criteria

Eligibility criteria included previously untreated patients with pathologically proven NSCLC with clinical tumor-node-metastasis system Stage III, and pathologic N2 was also required for Stage

Reprint requests to: Satoshi Ishikura, M.D., Radiation Oncology Division, National Cancer Center Hospital East, 6-5-1 Kashiwanoha, Kashiwa 277-8577, Japan. Tel: (+81) 4-7133-1111; Fax: (+81) 4-7131-4724; E-mail: sishikur@east.ncc.go.jp

This study was presented in part at the 38th Annual Meeting of ASCO in Orlando, Florida, May 18–21, 2002.

Acknowledgment—We thank Mrs. Fumiko Ko for her contribution to data management.

Received Mar 29, 2004, and in revised form Jul 9, 2004. Accepted for publication Jul 13, 2004.

IIIA; age, 20 to 74 years; performance status (PS) (based on Eastern Cooperative Oncology Group [ECOG] scale) 0 to 1; measurable disease; adequate hematologic (WBC count ≥4,000/mm^3, platelet count ≥100,000/mm^3, and hemoglobin ≥9.5 g/dL), hepatic (AST and ALT level ≤2 times the upper limit of normal and total bilirubin level ≤ the upper limit of normal), and renal (creatinine ≤1.2 mg/dL and creatinine clearance ≥60 mL/min) functions; PaO_2 ≥70 torr; no pleural and pericardial effusion; radiation field encompassed one-half or less of the ipsilateral lung; and no serious comorbidity. All patients signed written informed consent in accordance with our institutional review board.

Pretreatment evaluation included history and physical examination; serum chemistries (lactate dehydrogenase, alkaline phosphatase, AST, ALT, bilirubin, albumin, creatinine, and calcium); chest radiograph; CT scan of the chest; ultrasound of the abdomen; MRI or CT scan of the brain; and bone scintigraphy.

Treatment details

The treatment consisted of 2 cycles of CDDP 80 mg/m^2 on Day 1 and vinorelbine (VNR) 25 mg/m^2 on Days 1 and 8 every 3 weeks followed by HART; 3 times a day with minimal interval of 4 hours for a total dose of 57.6 Gy in 36 fractions over 2.5 weeks.

Radiation therapy was started after the patient recovered from the toxicity of chemotherapy and was delivered with megavoltage equipment. Lung heterogeneity corrections were not used. The first and third fraction of each day consisted of anterior-posterior opposed fields that encompassed the primary tumor, the metastatic lymph nodes, and the regional lymph nodes with a 1.5 to 2-cm margin. The fraction size was 1.5 Gy. Regional nodes excluding the contralateral hilar and supraclavicular nodes were included in these fractions. However, lower mediastinal nodes were included only if the primary tumor was located in the lower lobe of the lung. The second fraction of each day consisted of bilateral oblique fields that encompassed the primary tumor and the metastatic lymph nodes with a 1.5 to 2-cm margin; the fraction size was 1.8 Gy. Attempts were made to design the field of the second fraction to minimize the irradiated volume of the esophagus without compromising the margin around the tumor or spinal cord.

Toxicity assessment

Patients were observed weekly during treatment to monitor toxicity. Toxicity was graded according to the National Cancer Institute Common Toxicity Criteria (version 2.0). Late toxicity was graded according to the Radiation Therapy Oncology Group (RTOG)/European Organization for Research and Treatment of Cancer late radiation morbidity scoring scheme. Late toxicity was defined as that occurring more than 90 days after treatment initiation.

Follow-up evaluation

The following evaluations were performed until disease progression every 2 months for the first year, every 3 months for the second year, and every 6 months thereafter: physical examination, toxicity assessment, and chest radiograph. CT scan of the chest was performed at 1, 3, 6, 9, 12, 18, and 24 months after the treatment and when indicated thereafter. Restaging at 6 months after the treatment was also performed with ultrasound of the abdomen, MRI or CT scan of the brain, and bone scintigraphy.

Response assessment

Complete response (CR) was defined as complete disappearance of all measurable and assessable lesions for ≥4 weeks, partial response (PR) was defined as a decrease of 50% or more from baseline in the sum of products of perpendicular diameters of all measurable lesions for ≥4 weeks, and progressive disease (PD) was defined as an increase of 25% or more from baseline in the sum of products of perpendicular diameters of all measurable lesions or the appearance of any new lesion. Stable disease was defined as the remainder of evaluable patients without CR, PR, or PD.

Pattern of failure

Patterns of failure were defined as first site of failure. Local/regional failure included the primary tumor and regional lymph nodes. Distant failure included any site beyond the primary tumor and regional lymph nodes.

Statistics

A Simon's two-stage optimal design was used for this study with the assumption that a protocol compliance rate of less than 60% would not be feasible, and protocol compliance rate of 80% or greater with α error of 0.10 and β error of 0.10 would warrant further investigation of this regimen. In the first stage, 11 assessable patients were entered. If fewer than 7 patients completed the treatment, accrual would be stopped with the conclusion that the regimen was not feasible for further investigation. If 7 or more patients completed the treatment, an additional 27 patients would be accrued in the second study. According to this design, this study would be determined to be feasible and be proceeded to a multicenter Phase II study if 27 patients completed the treatment. The actuarial median survival time and 2-year survival were estimated by the Kaplan–Meier method (11).

RESULTS

Patient population

Between July 1999 and March 2001, 30 patients were enrolled in the study. The accrual was stopped, because 29 of 30 patients completed the treatment, and conclusions could be drawn at that time. The patients' median age was 64 years (range, 46–73 years), 24 were male, and 6 were female. The patient and tumor characteristics are summarized in Table 1.

Treatment compliance and toxicity

All patients completed 2 cycles of induction chemotherapy. Six of 30 patients required dose modification, and 13 patients had treatment delay. The median time to start of HART from start of chemotherapy was 49 days (range, 41–62 days). Twenty-nine of 30 patients completed HART, and the median overall treatment time of HART was 17 days (range, 16–22 days). In total, 29 of 30 patients (97%; 95% confidence interval [CI], 83–100%) completed this combined treatment.

The toxicity profile of the treatment is shown in Tables 2 and 3. Common Grade 3 or greater acute toxicities were neutropenia, 25 (83%); infection, 5 (17%); esophagitis, 5 (17%); and radiation pneumonitis, 3 (19%). There were 2 cases of treatment-related death due to radiation pneumonitis. As of the date of this analysis, 2 cases with Grade

Table 1. Patient and tumor characteristics

Number of patients	30
Age	
Median	64
Range	46–73
Gender	
Male	24
Female	6
Performance status	
0	8
1	22
Weight loss	
<5%	25
≥5%	5
Tumor and lymph nodes	
T1N2	3
T1N3	1
T2N2	5
T2N3	5
T3N2	1
T4N0	1
T4N1	4
T4N2	9
T4N3	1
Stage	
IIIA	9
IIIB	21
Histology	
Squamous	13
Nonsquamous	17

3 s.c. tissue fibrosis and 1 case with spontaneous rib fracture were observed as late toxicities.

Response and survival

Of 30 patients, 2 achieved CR, and 23 achieved PR with a response rate of 83% (95% CI, 65–94%). Five patients remained in a stable disease state, and there were no PD patients. With a median follow-up period of 40 months for surviving patients, the median survival and the 2-year and 3-year survivals (Fig. 1) were 24 months (95% CI, 13–34 months), 50% (95% CI, 32–68%), and 32% (95% CI, 15–49%), respectively. The median progression-free survival and the 1-year progression-free survival (Fig. 2) were 10 months (95% CI, 8–20 months) and 47% (95% CI, 29–65%), respectively.

Pattern of failure

At the time of this analysis, 22 of 30 patients (73%) showed tumor progression, 2 patients (7%) had died as a result of treatment, and 6 patients (20%) were alive without disease progression. The patterns of first failure were as follows: local/regional only, 13 (43%); local/regional and distant, 4 (13%); distant only, 5 (17%).

DISCUSSION

In the 1970s, treatment of locally advanced NSCLC was by conventional radiotherapy alone. In the 1980s, sequential chemotherapy and conventional radiotherapy

Table 2. Hematologic toxicities (n = 30)*

	Grade					
	0	1	2	3	4	≥Grade 3 (%)
Leukopenia	1	3	8	16	2	18 (60)
Neutropenia	3	0	2	6	19	25 (83)
Thrombocytopenia	20	7	1	2	0	2 (7)
Anemia	1	10	16	3	0	3 (10)

* National Cancer Institute–Common Toxicity Criteria version 2.

were revealed to be superior to conventional radiotherapy alone. In the 1990s, optimal sequences of chemoradiotherapy and radiation fractionation were investigated. The West Japan Lung Cancer Group compared sequential vs. concurrent radiotherapy with induction CDDP, vindesine, and mitomycin (7). In an RTOG 9410 trial, induction CDDP and vinblastine plus sequential standard radiotherapy, CDDP and vinblastine plus concurrent standard radiotherapy, and CDDP and etoposide plus concurrent twice-daily hyperfractionated radiotherapy were compared (8). Both trials showed similar results; concurrent chemoradiotherapy was superior to the sequential approach and achieved 5-year survivals for concurrent and sequential approach of approximately 20% and 10%, respectively. However, twice-daily hyperfractionated radiotherapy, which seemed to be promising in a preceding RTOG 9015 trial (12), failed to show a survival advantage over standard once-daily radiotherapy, and concurrent chemotherapy and once-daily radiotherapy is the standard of care today. Recently, a Czech randomized Phase II trial (13) suggested a similar advantage of the concurrent approach using CDDP and VNR, a newer cytotoxic agent. However, there remains some argument that newer cytotoxic agents cannot be delivered as full-dose chemotherapy with concurrent radiotherapy, and the survival advantage of newer cytotoxic agents over old ones has not yet been demonstrated in Stage III NSCLC patients. The optimal schedule and fractionation of thoracic radiotherapy in combination with chemotherapy also remains to be determined.

Another promising regimen was altered fractionation of radiotherapy such as CHART or HART, 3 times a day with a fraction interval of 4 to 6 hours over 2.5 weeks or less. CHART was developed at Mount Vernon Hospital, United Kingdom, in the 1980s. It was designed to combine both a shortening of the overall treatment time of radiotherapy, which is analogous to the concept of dose intensification of cytotoxic chemotherapy, and a reduction in dose per fraction. The rationale was to overcome accelerated repopulation of the tumor during the course of radiotherapy, which may lead to local failure, and to reduce normal tissue toxicities that depend on the dose per fraction. After the results of a randomized trial that showed survival benefits of CHART over conventional

Table 3. Nonhematologic toxicities (n = 30)*

	Grade						
	0	1	2	3	4	5	≥Grade 3 (%)
Acute toxicity							
Nausea	7	16	4	3	0	0	3 (10)
Vomiting	23	3	4	0	0	0	0
Infection	20	3	2	5	0	0	5 (17)
Esophagitis	1	11	13	4	1	0	5 (17)
Pneumonitis	18	4	5	1	0	2	3 (10)
Late radiation morbidity†							
Esophagus	26	1	0	0	0	0	0
Heart	26	0	1	0	0	0	0
Lung	9	13	5	0	0	0	0
Subcutaneous tissue	17	6	2	2	0	0	2 (7)
Bone	26	0	0	0	1	0	1 (3)

* National Cancer Institute–Common Toxicity Criteria version 2.
† Three patients died within 90 days of the beginning of radiotherapy.

radiotherapy (9), the Department of Health in the United Kingdom recommended CHART as the radiotherapy schedule of choice in inoperable NSCLC, and a CHART implementation group was formed to facilitate its introduction throughout the United Kingdom (14). There were difficulties in changing departmental working hours and a lack of sufficient financial support in UK hospitals to introduce CHART into routine practice (15), although it was suggested that CHART gave more benefit than any sequential combination of conventional radiotherapy and chemotherapy with minimally increased toxicity. To make the accelerated regimen more widely applicable, Continuous Hyperfractionated Accelerated Radiotherapy Week-End Less (CHARTWEL) and HART were introduced and were found to be as effective as CHART. Both CHARTWEL and HART showed improved survival over conventional radiotherapy, but the local tumor control was still unsatisfactory. Radiation dose escalation and use of chemotherapy combined with CHARTWEL/HART were also investigated to improve the local control and survival. Saunders *et al.* (16) reported on CHARTWEL combined with induction chemotherapy (17). In that study, 113 patients were enrolled, and dose escalation from 54 Gy to 60 Gy with or without chemotherapy was successfully achieved. Locoregional control at 2 years was 37% and 55% for CHARTWEL 54 Gy and 60 Gy alone, respectively, compared with 72% in those treated with 60 Gy and induction chemotherapy. These results suggested that chemotherapy improved locoregional control, but unfortunately they failed to show a statistically significant survival advantage, because of the relatively small number of patients and imbalanced tumor characteristics enrolled in each arm. The advantage of dose-escalated CHARTWEL against conventional radiotherapy is currently being investigated in a German Phase

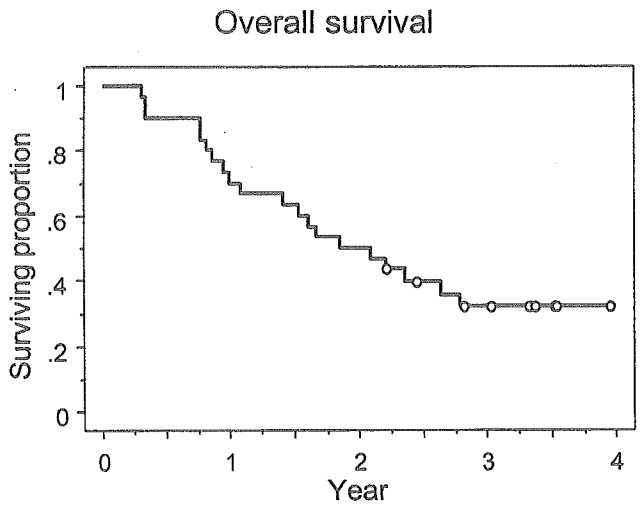

Fig. 1. Overall survival for all patients enrolled in this study.

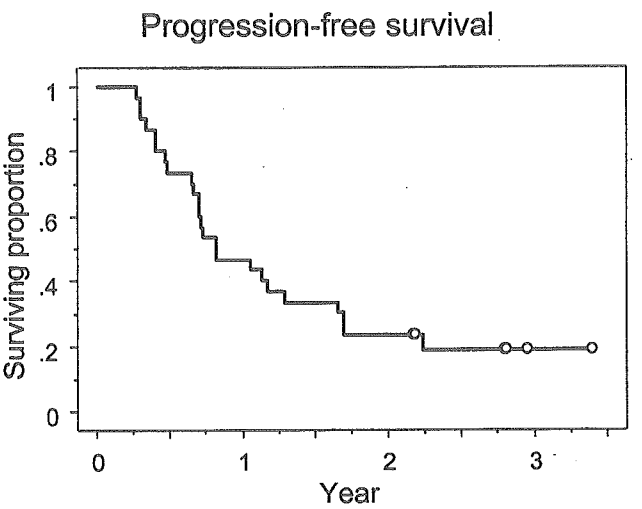

Fig. 2. Progression-free survival for all patients enrolled in this study.

III trial (18). Belani *et al.* reported the results of a randomized Phase III trial (19) that compared conventional radiotherapy with HART after induction chemotherapy (ECOG 2597). This study randomized 119 patients and unfortunately was closed because of slow accrual, but the results were provocative: The median survival time and the 2-year survivals for conventional radiotherapy and HART were 13.7 months and 33% vs. 22.2 months and 48%, respectively. These results seemed to be reliable despite the modest number of patients, because the median survival time of 13.7 months for the conventional radiotherapy arm was similar to that of a sequential chemoradiotherapy trial (2). The optimum chemotherapy regimen in combination with radiotherapy has not yet been determined, and we used a CDDP/VNR regimen instead of the carboplatin/paclitaxel regimen used in the ECOG 2597 trial. Both regimens are standards for advanced-stage NSCLC (20, 21). The compliance and toxicity profiles of chemotherapy in our study were acceptable, the incidence of esophagitis after HART was less than we expected, and the survival figure was nearly identical to that of the ECOG 2597 trial. This suggests that HART after induction CDDP/VNR or carboplatin/paclitaxel can achieve reproducible and promising results.

The pattern of failure in our study showed that local failure was still high (17 of 30, 57%) compared with distant metastasis (9 of 30, 30%), and further improvement of local control is needed. Future directions may include further dose intensification of radiotherapy and introduction of molecular-targeted agents. Recent innovation of information technology has made it possible to use sophisticated three-dimensional conformal radiotherapy (3DCRT). This can deliver intensified radiation doses to the tumor while minimizing the doses to the normal tissues that prevented further dose escalation using conventional two-dimensional radiotherapy. There have been several reports evaluating dose-intensified 3DCRT (22–25), and the technique is now under investigation in combination with cytotoxic chemotherapy in the Radiation Therapy Oncology Group trial (RTOG L-0117). Currently, molecular-targeted agents are being investigated most enthusiastically in Phase II and Phase III trials (26–29). It will be determined in the near future whether or not the combination of these agents has a survival impact. However, the optimal combination of these agents, newer cytotoxic agents, radiation fractionation, and 3DCRT will still need to be determined. Further investigation employing dose-intensified radiotherapy will be necessary to make a great leap in the treatment of locally advanced NSCLC.

REFERENCES

1. The editorial board of the cancer statistics in Japan (ed). Cancer statistics in Japan 2003. Foundation for promotion of cancer research. http://www.ncc.go.jp/en/statistics/2003/data03.pdf.
2. Dillman RO, Herndon J, Seagren SL, *et al.* Improved survival in stage III non-small-cell lung cancer: Seven-year follow-up of cancer and leukemia group B (CALGB) 8433 trial. *J Natl Cancer Inst* 1996;88:1210–1215.
3. Non-small Cell Lung Cancer Collaborative Group. Chemotherapy in non-small cell lung cancer: A meta-analysis using updated data on individual patients from 52 randomised clinical trials. *Br Med J* 1995;311:899–909.
4. Schaake-Koning C, van den Bogaert W, Dalesio O, *et al.* Effects of concomitant cisplatin and radiotherapy on inoperable non-small-cell lung cancer. *N Engl J Med* 1992;326:524–530.
5. Sause WT, Scott C, Taylor S, *et al.* Radiation Therapy Oncology Group (RTOG)88–08 and Eastern Cooperative Oncology Group (ECOG) 4588: Preliminary results of a phase III trial in regionally advanced, unresectable non-small-cell lung cancer. *J Natl Cancer Inst* 1995;87:198–205.
6. Sause W, Kolesar P, Taylor S, *et al.* Final results of phase III trial in regionally advanced unresectable non-small-cell lung cancer: Radiation Therapy Oncology Group, Eastern Cooperative Oncology Group, and Southwest Oncology Group. *Chest* 2000;117:358–364.
7. Furuse K, Fukuoka M, Kawahara M, *et al.* Phase III study of concurrent versus sequential thoracic radiotherapy in combination with mitomycin, vindesine, and cisplatin in unresectable stage III non-small-cell lung cancer. *J Clin Oncol* 1999; 17:2692–2699.
8. Curran W, Scott C, Langer C, *et al.* Long-term benefit is observed in a phase III comparison of sequential vs concurrent chemo-radiation for patients with unresected stage III NSCLC: RTOG 94–10 [Abstract]. *Proc Am Soc Clin Oncol* 2003;22:621a.
9. Saunders M, Dische S, Barrett A, *et al.* Continuous, hyperfractionated, accelerated radiotherapy (CHART) versus conventional radiotherapy in non-small cell lung cancer: Mature data from the randomised multicentre trial. *Radiother Oncol* 1999;52:137–148.
10. Mehta MP, Tannehill SP, Adak S, *et al.* Phase II trial of hyperfractionated accelerated radiation therapy for nonresectable non-small-cell lung cancer: Results of Eastern Cooperative Oncology Group 4593. *J Clin Oncol* 1998;16:3518–3523.
11. Kaplan EL, Meier P. Nonparametric estimation from incomplete observations. *J Am Stat Assoc* 1958;53:457–481.
12. Byhardt RW, Scott CB, Ettinger DS, *et al.* Concurrent hyperfractionated irradiation and chemotherapy for unresectable nonsmall cell lung cancer. Results of Radiation Therapy Oncology Group 90–15. *Cancer* 1995;75:2337–2344.
13. Zemanova M, Petruzelka L, Zemanova M. Concurrent versus sequential radiochemotherapy with vinorelbine plus cisplatin (V-P) in locally advanced non-small cell lung cancer. A randomized phase II study [Abstract]. *Proc Am Soc Clin Oncol* 2002;21:290a.
14. Macbeth F. An uncharted country. *Clin Oncol (R Coll Radiol)* 1999;11:71–72.
15. Saunders MI. Programming of radiotherapy in the treatment of non-small-cell lung cancer—a way to advance care. *Lancet Oncol* 2001;2:401–408.
16. Saunders MI, Rojas A, Lyn BE, *et al.* Dose-escalation with CHARTWEL (Continuous Hyperfractionated Accelerated Radiotherapy Week-End Less) combined with neo-adjuvant chemotherapy in the treatment of locally advanced non-small cell lung cancer. *Clin Oncol* 2002;14:352–360.
17. Bentzen SM, Saunders MI, Dische S. From CHART to

CHARTWEL in non-small cell lung cancer: Clinical radiobiological modelling of the expected change in outcome. *Clin Oncol* 2002;14:372–381.
18. Baumann M, Herrmann T, Matthiessen W, *et al.* CHART-WEL-Bronchus (ARO 97–1): A randomized multicenter trial to compare conventional fractionated radiotherapy with CHARTWEL radiotherapy in inoperable non-small-cell bronchial carcinoma. *Strahlenther Onkol* 1997;173:663–667.
19. Belani CP, Wang W, Johnson DH, *et al.* Induction chemotherapy followed by standard thoracic radiotherapy (Std. TRT) vs. hyperfractionated accelerated radiotherapy (HART) for patients with unresectable stage IIIA & B non-small cell lung cancer (NSCLC): Phase III study of the Eastern Cooperative Oncology Group (ECOG 2597) [Abstract]. *Proc Am Soc Clin Oncol* 2003;22:622a.
20. Kelly K, Crowley J, Bunn PA, *et al.* Randomized phase III trial of paclitaxel plus carboplatin versus vinorelbine plus cisplatin in the treatment of patients with advanced non-small-cell lung cancer: A Southwest Oncology Group Trial. *J Clin Oncol* 2001;19:3210–3218.
21. Pfister DG, Johnson DH, Azzoli CG, *et al.* American Society of Clinical Oncology treatment of unresectable non–small-cell lung cancer guideline: Update 2003. *J Clin Oncol* 2004;22:330–353.
22. Graham MV, Winter K, Purdy JA, *et al.* Preliminary results of a Radiation Therapy Oncology Group trial (RTOG 9311), a dose escalation study using 3D conformal radiation therapy in patients with inoperable nonsmall cell lung cancer [Abstract]. *Int J Radiat Oncol Biol Phys* 2001;51:20S.
23. Rosenzweig KE, Sim SE, Mychalczak B, *et al.* Elective nodal irradiation in the treatment of non-small-cell lung cancer with three-dimensional conformal radiation therapy. *Int J Radiat Oncol Biol Phys* 2001;50:681–685.
24. Hayman JA, Martel MK, Ten Haken RK, *et al.* Dose escalation in non–small-cell lung cancer using three-dimensional conformal radiation therapy: Update of a phase I trial. *J Clin Oncol* 2001;19:127–136.
25. Thirion P, Mc Gibney C, Holmberg O, *et al.* 3-dimensional conformal radiation therapy (3DCRT) permits radiobiological dose escalation for non-small-cell lung cancer (NSCLC): Preliminary results of a phase I/II trial [Abstract]. *Proc Am Soc Clin Oncol* 2001;20:344a.
26. Gandara DR, Chansky K, Albain KS, *et al.* Consolidation docetaxel after concurrent chemoradiotherapy in stage IIIB non-small-cell lung cancer: Phase II Southwest Oncology Group Study S9504. *J Clin Oncol* 2003;21:2004–2010.
27. Milas L, Fan Z, Andratschke NH, *et al.* Epidermal growth factor receptor and tumor response to radiation: In vivo preclinical studies. *Int J Radiat Oncol Biol Phys* 2004;58:966–971.
28. Ochs JS. Rationale and clinical basis for combining gefitinib (IRESSA, ZD1839) with radiation therapy for solid tumors. *Int J Radiat Oncol Biol Phys* 2004;58:941–949.
29. Choy H, Milas L. Enhancing radiotherapy with cyclooxygenase-2 enzyme inhibitors: A rational advance? *J Natl Cancer Inst* 2003;95:1440–1452.

TECHNICAL NOTE

Radiation Medicine: Vol. 23 No. 3, 216–219 p.p., 2005

Simple Technique to Visualize Random Set-up Displacements Using a Commercially Available Radiotherapy Planning System

Hiromichi Ishiyama,* Masashi Kitano,* Yuzuru Niibe,* Mineko Uemae, and Kazushige Hayakawa***

Purpose: To visualize random set-up displacements in isodose distribution images, we introduce a simple technique using a commercially available radiotherapy planning system (RTP).
Materials and Methods: A distribution of set-up displacement is known to be compatible with that of a Gaussian distribution. Based on that assumption, 41 intentionally misaligned beams with 1-mm intervals were planned in the respective weights according to Gaussian distribution. "Modified" isodose distributions were then visualized using a commercially available RTP. In the next step, only two beams misaligned with one standard deviation (SD) of the Gaussian distribution were used in place of 41 beams, as a large number of beams increases the workload and is unsuitable for clinical use. Differences between the two versions of isodose distribution images were assessed visually.
Results: In modified dose distribution images, the edge of distribution was dull compared to normal images. These images show that the larger SD of set-up displacement dulls the edge of dose distribution. Images from two beams were not significantly different to those from 41 beams.
Conclusion: Using this technique, the impact of random set-up displacements was effectively reflected in isodose distribution images.

Key words: set-up displacement, radiotherapy, treatment simulation

Introduction

Geometrical uncertainties in radiotherapy cause differences between intended and actual delivered dose distributions. One of the major causes of uncertainties is set-up displacement.

Set-up displacement can involve systematic and/or random displacement.[1] Systematic displacement comprises the same displacement for each fraction of treatment, whereas random displacement varies from day to day. By measuring set-up displacement several times, the typical sizes of systematic and random displacement can be determined,[2] and the standard deviation (SD) of set-up displacement is reportedly 1.0-5.0 mm for currently applied treatment techniques.[3] In addition, distributions of set-up displacements for all three directions are compatible with that of a Gaussian distribution because of a large number of set-up procedures,[4] and the average and SD of Gaussian distributions are compatible with systematic and random set-up displacement, respectively.

Usually, the margin to expand clinical target volume (CTV) to obtain sufficient tumor coverage is planned empirically by physicians. However, empirical methods could represent a cause of decreased tumor control and increased complications involving normal tissues. In particular, with the recent advent of computed tomography (CT) simulations, isodose distribution images are crucial because of heavy dependence on them by physicians and physicists. For more precise and reasonable planning, we believe that visualization of set-up displacement in isodose distribution images is needed.

This report introduces and assesses a simple technique for visualizing random set-up displacements using a commercially available radiotherapy planning system (RTP).

Received July 16, 2004; revision accepted October 8, 2004.
*Department of Radiology, Kitasato University School of Medicine
**Division of Radiation Oncology, Kitasato University Hospital
Reprint requests to Hiromichi Ishiyama, M.D., Department of Radiology, Kitasato University Hospital, 1-15-1 Kitasato, Sagamihara, Kanagawa 228-8555, JAPAN.

Materials and Methods

Phantom study

A solid water phantom (Solid Water®, Gammex RMI, Middleton, WI, USA) was scanned with a CT simulator using a slice thickness and interval of 5 mm. All images were transferred to a three-dimensional treatment planning system (Pinnacle³®, version 6.5b, ADAC Co., USA). Anterior 10 cm×10 cm irradiations with 4 MV photons were planned. Isodose curves of 110%, 107%, 100%, 95%, 90%, 80%, 70%, 60%, 50%, 40%, 30%, 20%, and 10% relative to an isocenter dose were displayed as a "normal" isodose distribution.

On the assumption that translations of set-up displacements would occur between –20 mm and +20 mm, 41 intentionally misaligned beams were planned with 1-mm intervals along the horizontal axis. Considering the isodose distribution of a total treatment course all at once, the number of fractions at each misaligned beam could be considered the weight of those respective beams. To calculate the weight of each misaligned beam, values of density function of the Gaussian distribution were used. The operational window of Excel software (Microsoft, USA) was used for value calculations (Fig. 1). The average of Gaussian distributions was set on 0 mm, and SDs were set on 1-5 mm, with 1-mm intervals. The five Gaussian distributions were therefore calculated for different SDs and were visualized as "modified" isodose distributions.

Modified isodose distribution images were visually compared with normal isodose distribution images.

Simplification for clinical use

Although a greater number of intentionally misaligned beams makes the Gaussian distribution smoother and more accurate, the workload of operators would be significantly increased. We therefore needed to decrease the number of misaligned beams for clinical use. In principle, as few as two symmetric beams misaligned within 1 SD can be used as a substitute for the large number of misaligned beams, because SD is statistically defined in the literature as a "standard" of deviations. Modified isodose distribution images from two beams were visually compared with those from 41 beams.

Results

"Normal" and "modified" isodose distributions were calculated from 41 beams or two beams (Fig. 2). In modified images, the edge of the distribution was dull

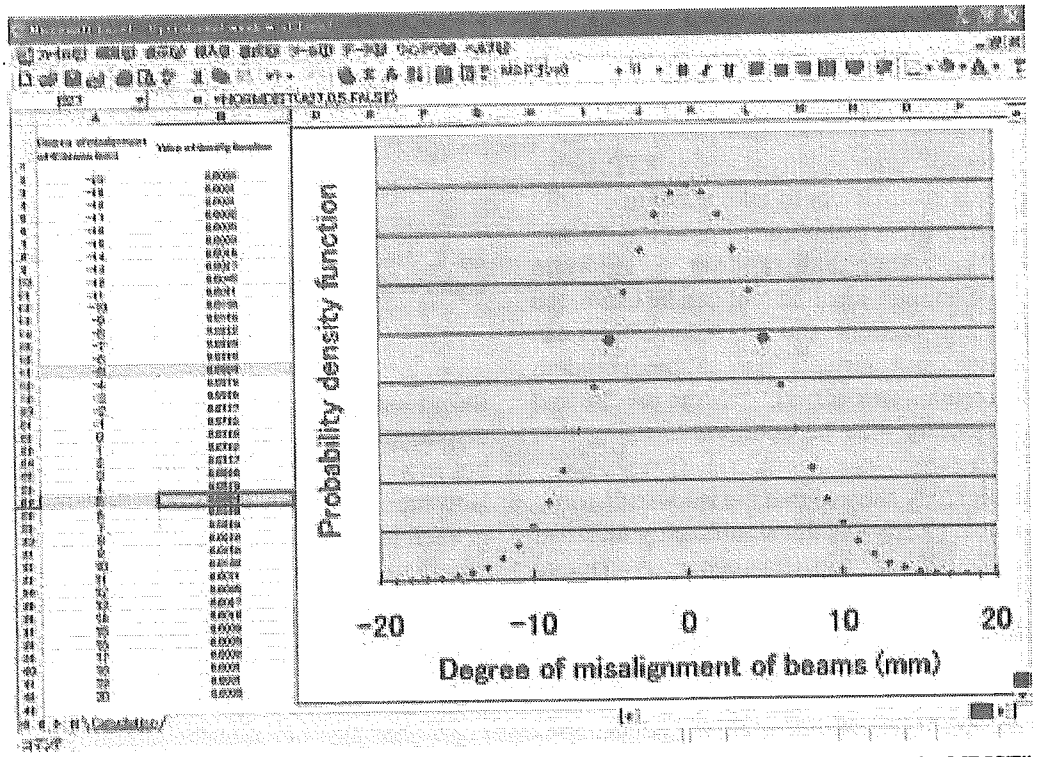

Fig. 1. Values of density function of the Gaussian distribution were calculated using the "NORMDIST" function of Excel software (Microsoft). For calculating the modified isodose distributions from two beams, a pair of symmetric beams misaligned with 1 SD was used (large points in the distribution).

compared to normal images. These images show that a larger SD of set-up displacement dulls the edge of dose distribution. Isodose distribution based on 2 beams was not significantly different from that based on 41 beams.

Clinical case

A case involving prostatic cancer is shown in Fig. 3. The prostate and rectum were manually contoured and planned using a 4-field box technique with 10-MV photons. On the assumption that random set-up displacement within 5-mm SD occurred along all three axes, the isodose distribution image and dose-volume histogram were calculated. Although differences were relatively slight, the impact of random set-up displacement was reflected in both the isodose distribution image and dose-volume histogram.

Discussion

Detailed calculations based on dose coverage of the CTV have been given in a previous report.[5] According to this report, if the SD of systematic errors (Σ) and of random errors (ρ) are known for a specific patient group, the margin M to expand the CTV to a safe planning target volume (PTV) may be expressed as $M = 2\Sigma + 0.7\rho$. With this calculated margin, CTV would be covered with a 95% isodose curve. However, to adapt this calculation to clinical use, manual input of tumor contours is essential. Due to the huge volume of CT data, manual input of all tumor contours for all cases is impractical.

The technique introduced in this report is useful for visually comprehending random set-up displacements, and allows the use of commercially available RTP. Using this technique, it is sufficient to take account of only systematic displacement that is constant during therapy and predictable, rather than random. Systematic displacement of an individual patient can be estimated during the first few fractions, and couch corrections can be applied for subsequent irradiations, although random displacements remain unchanged.[1,6-8] More precise and reasonable planning may be achievable using this technique.

Although this study showed that the isodose distribution based on two beams was not significantly different from that based on 41 beams in a homogeneous phantom study, different distributions may be shown in clinical use with electron density correction. There is need to take account of this point, and further examination is recommended.

Whatever is done to minimize geometrical uncertainties, inaccuracies are to some extent unavoidable. Once typical values for a specific group of patients are known, these should be included in treatment planning for individual patients from that group. Patient set-up displacement not only affects dose in the tumor region, but in neighboring, possibly critical, organs as well. However, the typical size of set-up displacement differs in each institution, as methods of patient fixation and set-up verification systems vary. In addition, beam profiles of linear accelerators differ in each institution. Simulations of data for typical set-up displacement therefore need to be performed at each institution. For this reason, availability of a simple, standard technique is crucial, and our technique can be applied to any institution. Using the technique introduced in this paper, the impact of random set-up displacements can be effectively reflected in isodose distribution images.

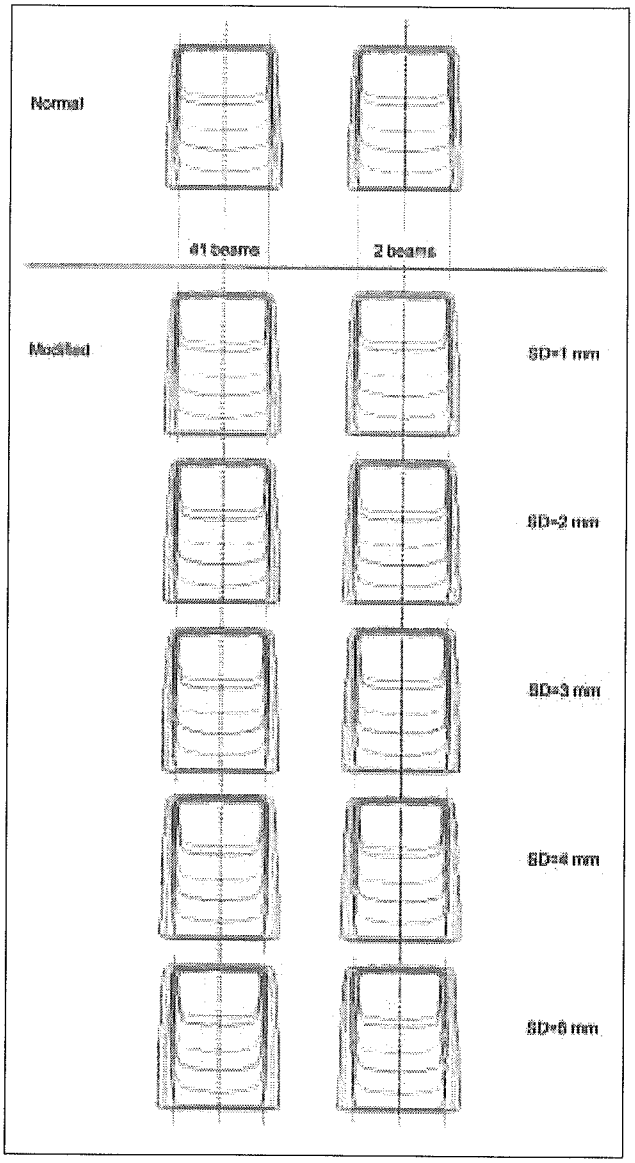

Fig. 2. Modified isodose distributions were calculated from two beams or 41 beams. The portal size was 10 cm×10 cm.

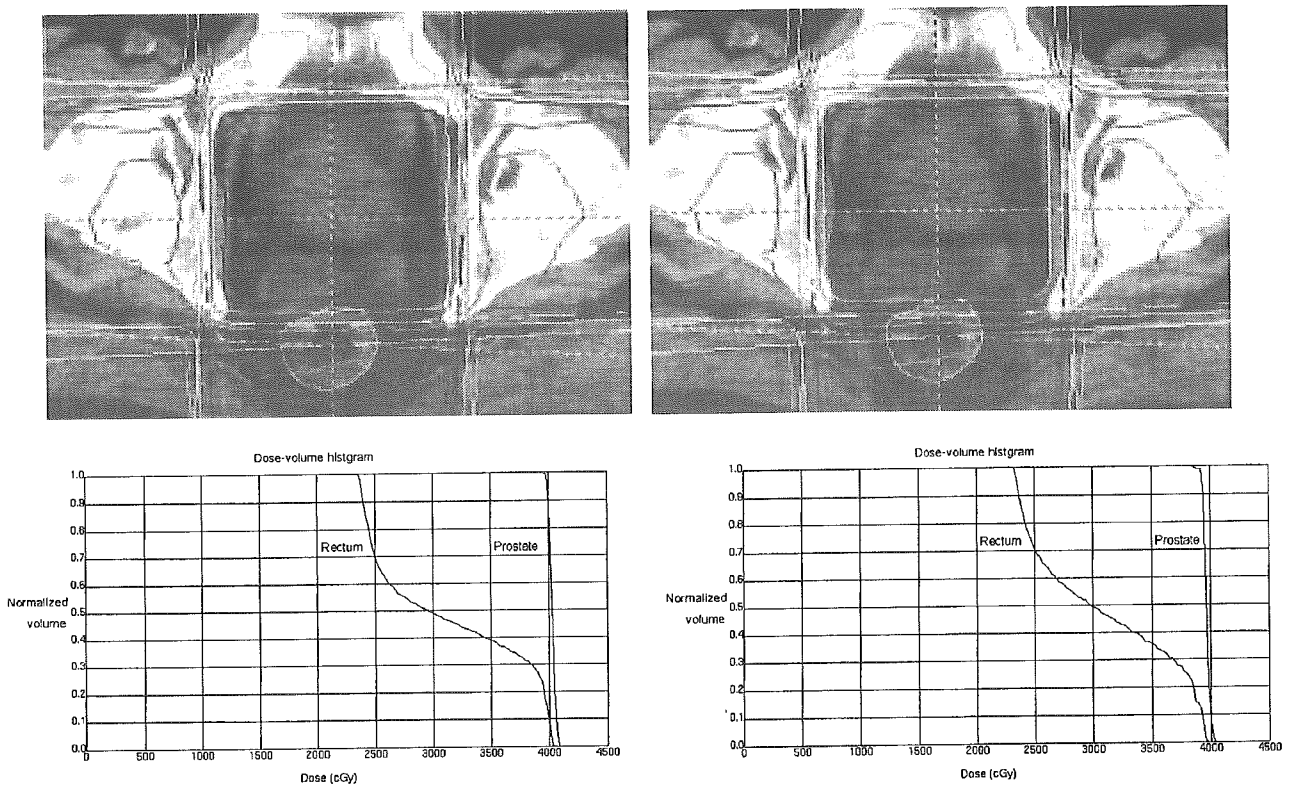

Fig. 3. Edge of the isodose distribution was sharp in normal distribution (A) and dull in modified distribution (B). Dose-volume histograms of the prostate and rectum reflect differences between normal (C) and modified (D) distributions.

A	B
C	D

ACKNOWLEDGEMENTS

This work was supported in part by Grant-in-Aid for Scientific Research from Japan Society for the Promotion of Science and the Ministry of Health, Labour and Welfare in Japan.

REFERENCES

1) Bel A, van Herk H, Bartelink H, Lebesque JV. A verification procedure to improve patient set-up accuracy using portal images. *Radiother Oncol*, 29: 253–260, 1993.
2) Bijhold J, Lebesque JV, Hart AA, Vijlbrief RE. Maximizing setup accuracy using portal images as applied to a conformal boost technique for prostatic cancer. *Radiother Oncol*, 24: 261–271, 1992.
3) Hurkmans CW, Remeijer P, Lebesque JV, Mijnheer BJ. Set-up verification using portal imaging; review of current clinical practice. *Radiother Oncol*, 58: 105–120, 2001.
4) Rudat V, Flentje M, Oetzel D, Menke M, Schlegel W, Wannenmacher M. Influence of the positioning error on 3D conformal dose distributions during fractionated radiotherapy. *Radiother Oncol*, 33: 56–63, 1994.
5) Stroom JC, de Boer HC, Huizenga H, Visser AG. Inclusion of geometrical uncertainties in radiotherapy treatment planning by means of coverage probability. *Int J Radiat Oncol Biol Phys*, 43: 905–919, 1999.
6) Yan DD, Wong JW, Gustafson G, Martinez A. A new model for "accept or reject" strategies in off-line and on-line megavoltage treatment evaluation. *Int J Radiat Oncol Biol Phys*, 31: 943–952, 1995.
7) Yan D, Wong J, Vicini F, *et al.* Adaptive modification of treatment planning to minimize the deleterious effects of treatment setup errors. *Int J Radiat Oncol Biol Phys*, 38: 197–206, 1997.
8) Boer HCJ, Heijmen BJM. A protocol for the reduction of systematic patient setup errors with minimal portal imaging workload. *Int J Radiat Oncol Biol Phys*, 50: 1350–1365, 2001.

Hepatoma-derived growth factor as a prognostic marker in completely resected non-small-cell lung cancer

TERUO IWASAKI[1], KATSUHIRO NAKAGAWA[1], HIDEJI NAKAMURA[4], YOSHIAKI TAKADA[2], KAORU MATSUI[3] and KUNIMITSU KAWAHARA[2]

Departments of [1]Respiratory Surgery, [2]Pathology and [3]Thoracic Malignancy, Osaka Prefectural Medical Center for Respiratory and Allergic Diseases (formerly Osaka Prefectural Habikino Hospital); [4]Division of Hepatobiliary and Pancreatic Medicine, Department of Internal Medicine, Hyogo College of Medicine, 1-1 Mukogawa-cho, Nishinomiya, Hyogo 663-8501, Japan

Received January 4, 2005; Accepted February 22, 2005

Abstract. Hepatoma-derived growth factor (HDGF), unrelated to hepatocyte growth factor, is a heparin-binding protein originally purified from human hepatoma HuH-7 cells. HDGF exhibits mitogenic activities for certain hepatoma cells, fibroblasts and vascular smooth muscle cells, and angiogenic activities through nuclear targeting. Recently, HDGF was found to be a mitogen for lung epithelial cells *in vitro* and *in vivo*. This suggests that HDGF may play a critical role in the development and progression of lung cancer. We investigated, immunohistochemically, the relationship between HDGF expression and clinicopathological variables, and the prognostic significance of HDGF in 102 patients with completely resected non-small-cell lung cancer (NSCLC: 70 adenocarcinomas and 32 squamous cell carcinomas). To address the mechanism of action of HDGF, we evaluated the contribution of HDGF to tumor cell proliferation and intratumor angiogenesis using anti-Ki-67 and anti-CD31 antibodies, respectively. HDGF expression was strongly detected in the nucleus of cancer cells; the HDGF-labeling index (LI) was 20-95% (median 64.5%). There was no significant association between HDGF-expression level and clinicopathological variables. Patients with NSCLC showing a high HDGF-LI (≥65%) had significantly worse overall and disease-free survivals than those with NSCLC showing a low HDGF-LI. Multivariate analysis revealed that HDGF is a significant independent prognostic factor, more powerful than pathological stage. Moreover, HDGF expression correlated with Ki-67-LI and intratumor microvessel density. We consider HDGF as a useful prognostic marker for patients with completely resected NSCLC and it may play a critical role in the pathobiology of lung cancer through its mitogenic and angiogenic activities.

Correspondence to: Dr Teruo Iwasaki, Department of Respiratory Surgery, Osaka Prefectural Medical Center for Respiratory and Allergic Diseases, 3-7-1 Habikino, Habikino-City, Osaka 583-8588, Japan
E-mail: teruteruah@m4.dion.ne.jp

Key words: hepatoma-derived growth factor (HDGF), non-small-cell lung cancer, prognostic factor, immunohistochemical study, microvessel density

Introduction

Hepatoma-derived growth factor (HDGF), unrelated to hepatocyte growth factor (HGF) produced by non-parenchymal cells, is a secretory heparin-binding protein that was purified from the conditioned medium of human hepatoma HuH-7 cells, and its cDNA was cloned from HuH-7 cells (1,2). HDGF represents a new family of growth factors called HDGF-related proteins (HRPs), including HRP1, HRP2, HRP3, HRP4 and p52/p75/lens epithelium-derived growth factor (LEDGF) (3). These proteins have in common the following characteristics: i) homology in the N-terminal amino acids [termed homologous to the amino terminus of HDGF (hath) region] containing a PWWP domain, which is suspected to play a role in cell growth and differentiation possibly by DNA binding, ii) bipartite nuclear localization signals, and iii) lack of signal peptides (3-5). Recent studies have shown that HDGF is an exogenous mitogen for HuH-7, Swiss 3T3 fibroblasts (2), endothelial cells (6-8), and vascular smooth muscle cells (9,10), and that nuclear targeting of HDGF is essential for its mitogenic activity (10,11).

As for roles of HDGF in tumor pathobiology, HDGF stimulates *in vitro* proliferation of hepatoma cells such as HuH-7, and antisense oligonucleotides of HDGF can suppress it (12). *In vivo*, HDGF induces tumorigenesis of NIH3T3 cells in nude mice through its angiogenic activity (7) and may also play an important role in the development and progression of hepatocellular carcinoma in humans and rodents on the basis that HDGF expression is higher in hepatoma cells than in the adjacent non-cancerous tissues (13).

Although HDGF was originally identified in hepatoma cells, HDGF and its mRNA are expressed in various normal adult tissues, including lung tissue (2,6,14). HDGF may be involved in fetal lung development (15). Recently, Mori *et al* (14) reported that HDGF is also a mitogen for lung epithelial cells *in vitro* and *in vivo*. Taken together, these findings suggest that HDGF may play a critical role in the development and progression of lung cancer.

The most common cancer in Japan today is lung cancer. Lung cancer was the leading indication for general thoracic

surgery (~43%) and more than 20,000 patients were operated on at Japanese institutions in 2002 (16). Non-small-cell lung carcinomas (NSCLC) represent 98% of all operable cases of lung cancer, and they are still associated with a poor prognosis, even when operable. Many molecular markers of prognosis have been studied, although the critical cause for the poor prognosis of patients with NSCLC remains to be determined.

In the present study, we investigate immunohistochemically the relationship between HDGF expression and clinicopathological variables and the prognostic significance of HDGF in NSCLC patients who underwent complete resection. Additionally, to address the mechanism of action of HDGF on lung cancer biology, we evaluated the contribution of HDGF to tumor cell proliferation and intratumor angiogenesis.

Materials and methods

Patients and tumors. Among patients with primary lung carcinoma who were operated on at the Osaka Prefectural Medical Center for Respiratory and Allergic Diseases (Osaka, Japan) from 1994 through 1997, one hundred and two patients underwent complete resection for adenocarcinoma (n=70) or squamous cell carcinoma (n=32) without previous chemotherapy or radiotherapy, and adequate paraffin-embedded tissue sections were available. These patients had no other form of malignancy. Tumor specimens were fixed in 10% formaldehyde solution, embedded in paraffin and microscopically examined after hematoxylin and eosin (HE) staining. Histological classification of tumors was based on the World Health Organization criteria. Visceral pleural involvement was classified according to the Japan Lung Cancer Society (17) as follows: P0, the tumor does not penetrate the elastic layer of the visceral pleura; P1, the tumor penetrates the elastic layer but is not exposed on the pleural surface; P2, the tumor is exposed on the pleural surface but does not involve adjacent anatomic structures; and P3, the tumor involves adjacent anatomic structures (18). A tumor larger than 3 cm in diameter or a P2 tumor of any size was defined as T2 classification. All tumors were staged according to the TNM pathological classification of the American Joint Committee on Cancer (AJCC) and the International Union Against Cancer (UICC) (19): 40 stage I (23 cases in stage IA and 17 cases in stage IB), 21 stage II (3 cases in stage IIA and 18 cases in stage IIB), 35 stage III (26 cases in stage IIIA and 9 cases in stage IIIB) and 6 stage IV (patients with a metastatic nodule in the ipsilateral non-primary-tumor lobe of the lung). The patients (69 men and 33 women) were between 40 and 80 years of age (mean 64 years) and grouped according to age as being either <70 or ≥70 years old. Smoking status was 0-232 (median 44.5) pack-year, and patients were divided into 2 groups: those who smoked <40 pack-year and those who smoked ≥40 pack-year. Survival was calculated from the day of surgery, and follow-up of the 102 patients ranged from 4.1 to 108.9 (median 61.3) months; 54 patients (52.9%), without exception, died of recurrence or metastasis of lung cancer during follow-up. Our study was carried out with the approval of the ethical committee of the Osaka Prefectural Medical Center for Respiratory and Allergic Diseases.

Immunohistochemical examination. Immunohistochemical staining for HDGF was performed essentially as previously described (7,12,14,20). The paraffin sections (4 μm thick) were deparaffinized, microwaved in 10 mmol/l citrate buffer (pH 6.0) and then immersed in methanol containing 0.3% hydrogen peroxide. Slides were blocked with normal goat serum and incubated with a 1:5,000 dilution of rabbit polyclonal IgG raised against C-terminus (231-240) of the human HDGF sequence for 30 min at room temperature. After washing the sections twice with phosphate-buffered saline, they were incubated with peroxidase-conjugated goat anti-rabbit immunoglobulin (Envision; Dako, Glostrup, Denmark) for 30 min at room temperature. After washing, diaminobenzidine tetrahydrochloride (DAB) solution was applied. The sections were then counterstained in hematoxylin. Specificity of the anti-HDGF antibody (Ab) had been previously demonstrated by Western blot analysis using recombinant human HDGF (14). Weak staining of smooth muscle cells and endothelial cells of blood vessels was used as the internal positive control. Negative controls were treated in the same way, but anti-HDGF Ab was replaced by non-immune rabbit serum. HDGF was detected mainly in the nucleus of cancer cells more strongly than in that of smooth muscle cells, and weakly in the cytoplasm of some cancer cells. HDGF immunoreactivity was judged positive when HDGF staining in the nucleus of tumor cells was equivalent to or stronger than that in the nucleus of smooth muscle cells. HDGF-labeling index (LI) was expressed as the proportion of cancer cells with positive HDGF nuclear reactivity.

Immunohistochemical staining for Ki-67 nuclear antigen was performed using a mouse monoclonal anti-human Ki-67 antigen Ab (MIB-1, DAKO) according to the manufacturer's instructions. Ki-67-LI was expressed as the proportion of Ki-67-positive cancer cells. For evaluation of HDGF- and Ki-67-LI, more than 1,000 cancer cells were counted in at least 5 representative areas without necrosis in each section. Intratumor angiogenesis was assessed by counting the microvessels detected with CD31 staining using a mouse monoclonal anti-human CD31 Ab (JC/70A, DAKO) according to the manufacturer's instructions. Intratumoral microvessel density (MVD) was calculated as the average value of microvessels/mm^2 using the criteria previously described elsewhere (21,22). After the area of highest vascularization was identified by scanning sections at low power, individual microvessel counts were determined at magnification x200 (0.95 mm^2 area) in 3 different fields under an Olympus microscope (Tokyo, Japan). All values determined by slide examination were presented by the median of scores evaluated by 3 investigators (Teruo Iwasaki, Yoshiaki Takada and Kunimitsu Kawahara).

Statistical analysis. The relationship between HDGF expression and clinicopathological variables [age, sex, smoking, tumor size, pathological stage, T-factor (classification), N-factor (classification), pleural involvement, vascular involvement, lymphatic involvement, histological type and degree of differentiation] was analyzed by the χ^2-test. The significance of differences in Ki-67-LI and MVD was tested by Student's t-test. The Kaplan-Meier method was used to estimate overall and disease-free survival as a function of time, and survival differences were analyzed by the log-rank test. Factors potentially related to overall and disease-free survival were analyzed by the Cox proportional-hazards model. For all

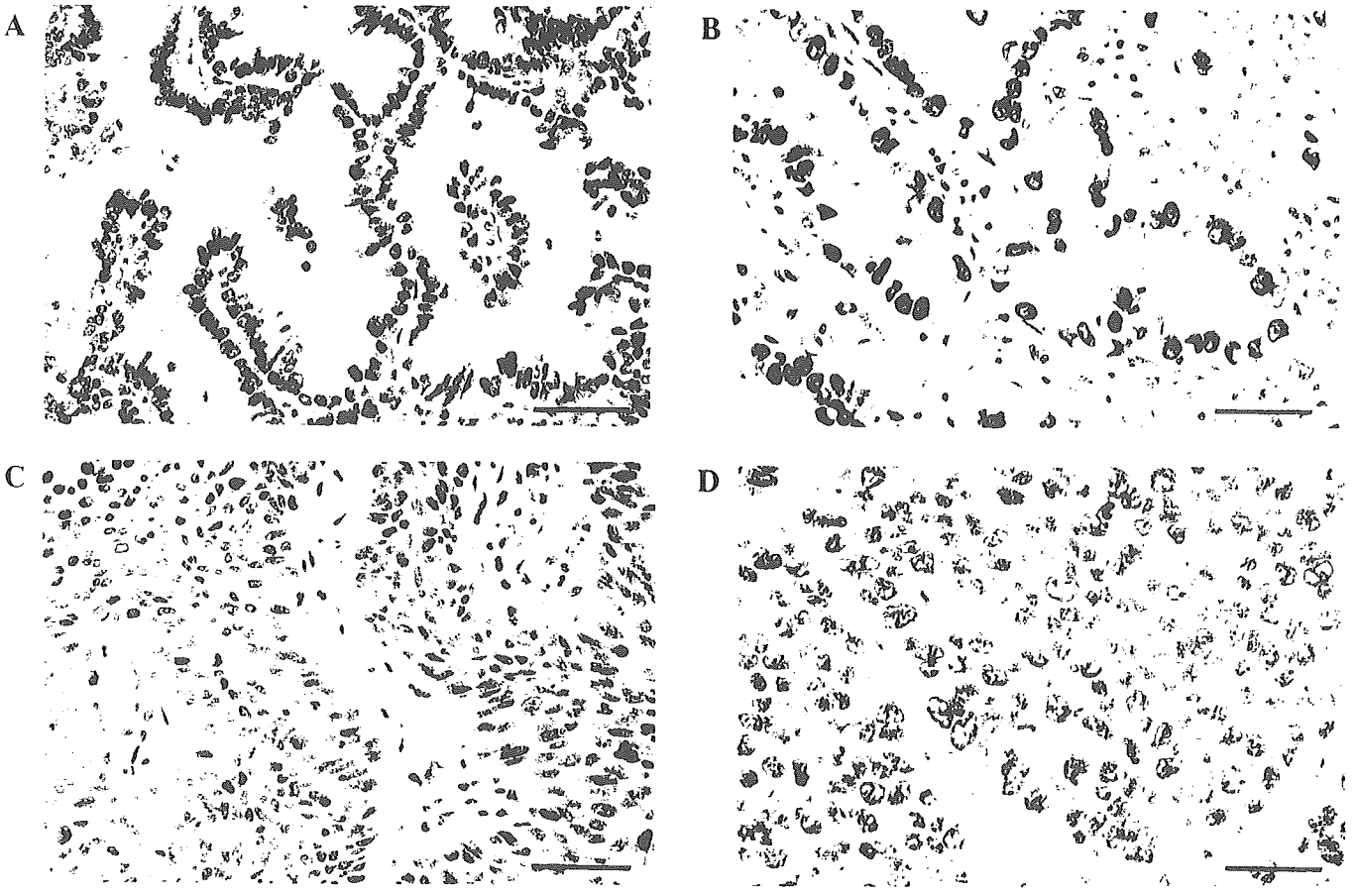

Figure 1. Representative photomicrographs of immunohistochemical staining of HDGF in adenocarcinoma (A and B) and squamous cell carcinoma (C and D) cases. HDGF is expressed weakly in the nucleus of <65% of tumor cells in A and C (defined as low HDGF-expression). To the contrary, HDGF staining was more intense in the nucleus and weak in the cytoplasm of ≥65% of tumor cells in B and D (defined as high HDGF-expression). Scale bars, 50 μm.

statistical analyses, the criterion of significance was defined as $P<0.05$.

Results

HDGF expression was detected in all tumor sections in various proportions. Many cancer cells exhibited strong HDGF-staining, mainly in the nucleus, and some cancer cells presented weak staining in the cytoplasm. Representative cases of adenocarcinoma and squamous-cell carcinoma are shown in Fig. 1. The median score of HDGF-LI in all cases was 64.5% (20-95%), and therefore we defined 65% as a cut-off for low (<65%, n=51) and high (≥65%, n=51) expression. Weak staining in the endothelial cells and smooth muscle cells in the vessels was used as the internal control as mentioned above. HDGF was also detected weakly in some of the non-cancerous type II pneumocytes and ciliated columnar epithelial cells (data not shown). These findings were consistent with those of a previous report on idiopathic pulmonary fibrosis (14).

The relationship between HDGF expression and clinicopathological variables (age, sex, smoking, tumor size, stage, T-factor, N-factor, pleural involvement, vascular involvement, lymphatic involvement, histology and differentiation) in all cases is summarized in Table I. There was no significant relationship between HDGF expression and any clinicopathological variable.

Kaplan-Meier overall and disease-free curves for HDGF expression dichotomized by the median level are shown in Figs. 2 and 3, respectively. Patients with lung cancer expressing high HDGF had a significantly worse overall and disease-free survival than those with lung cancer expressing low HDGF ($P=0.0004$ and $P=0.0005$ by the log-rank test, respectively). Among 102 patients, 25 received adjuvant therapy: radiotherapy was given to 6 patients and systemic chemotherapy including cisplatin or a combination of uracil and tegafur (UFT) was given to 19 patients. There was no significant difference in the proportion of patients who received adjuvant therapy between the 2 groups (13/51 in the low-HDGF group and 12/51 in the high-HDGF group, $P>0.99$).

In the univariate analysis of correlations between prognosis and potential prognostic factors evaluated (HDGF expression, adjuvant therapy and the 12 clinicopathological variables shown in Table I), vascular involvement, smoking, N-factor, tumor size, sex, pathological stage and HDGF were significant prognostic factors ($P<0.05$) for overall and disease-free survival. Adjuvant therapy was not a significant factor for overall ($P=0.580$) or disease-free ($P=0.536$) survival in this study. These 7 significant variables were entered into the Cox proportional-hazards model and multivariate analysis was performed (Table II). Pathological stage and HDGF-expression level were significant independent prognostic factors for overall and disease-free survival, and moreover HDGF had

Table I. Association between HDGF-expression and clinicopathological variables in all cases.

Variables	High-HDGF (%)	Low-HDGF	P-value[a]
Age			
<70 years	37 (50.0)	37	
≥70 years	14 (50.0)	14	>0.999
Sex			
Male	38 (55.1)	31	
Female	13 (39.4)	20	0.204
Smoking			
<40 pack-year	28 (54.9)	23	
≥40 pack-year	23 (45.1)	28	0.428
Tumor size			
≤30 mm	17 (40.5)	25	
>30 mm	34 (59.5)	26	0.159
pStage[b]			
Stage I + II	30 (49.2)	31	
Stage III + IV	21 (51.2)	20	>0.999
pT-factor[b]			
T1 + T2	42 (49.4)	43	
T3 + T4	9 (52.9)	8	>0.999
pN-factor[b]			
N0	25 (51.0)	24	
N1 + N2	26 (49.0)	27	>0.999
Pleural involvement[c]			
P0 + P1	40 (49.4)	41	
P2 + P3	11 (50.6)	10	>0.999
Vascular involvement			
v (-)	19 (48.7)	20	
v (+)	32 (50.8)	31	>0.999
Lymphatic involvement			
ly (-)	16 (50.0)	16	
ly (+)	35 (50.0)	35	>0.999
Histology[d]			
Ad	38 (54.3)	32	
Sq	13 (40.6)	19	0.286
Differentiation			
Well	25 (45.5)	30	
Moderate/poor	26 (55.3)	21	0.427

[a]χ^2-test. [b]According to the AJCC/UICC TNM pathological classification. pStage, pathological stage; pT, pathological tumor; pN, pathological lymph node; [c]According to the general rules for clinical and pathological record of lung cancer established by the Japan Lung Cancer Sosiety. [d]Ad, adenocarcinoma; Sq, squamous cell carcinoma.

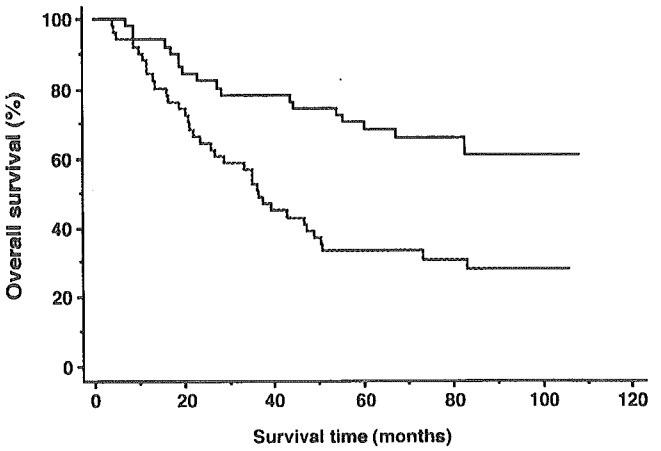

Figure 2. Kaplan-Meier analysis of the overall survival of NSCLC patients with low (a solid line) and high (a dotted line) HDGF-expression. P=0.0004 by the log-rank test.

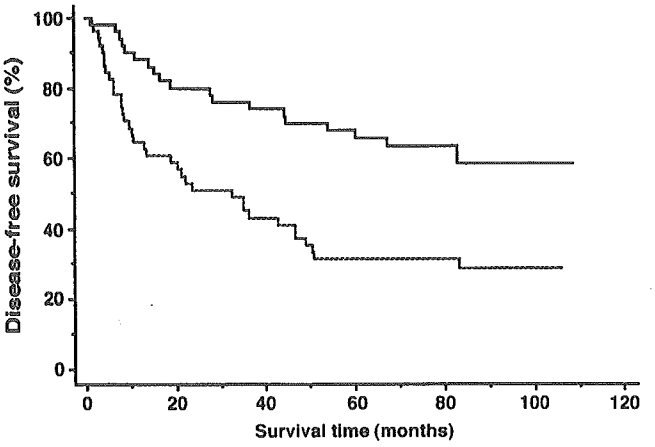

Figure 3. Kaplan-Meier analysis of the disease-free survival of NSCLC patients with low (a solid line) and high (a dotted line) HDGF-expression. P=0.0005 by the log-rank test.

higher risk-ratios than pathological stage for overall (2.976 versus 1.964) and disease-free survivals (2.970 versus 1.848).

The role of HDGF in the biological behavior of NSCLC remains to be fully elucidated. HDGF was very recently reported to be not only a mitogenic factor for lung epithelial cells but also an angiogenic factor (6,9,10,14). We, therefore, examined the relationship between HDGF-expression level and Ki-67-LI or MVD in serial sections. Ki-67-LI values for low and high HDGF-expressing cases were 19.3±14.3% and 34.1±17.7%, respectively (mean ± SD, P<0.00005 by Student's t-test). MVD values for low and high HDGF-expressing cases were 49.8±23.6 and 68.5±20.7 vessels/mm^2, respectively (mean ± SD, P<0.00005 by Student's t-test). These findings suggested that HDGF may promote the proliferation of tumor cells and intratumor angiogenesis in lung cancer.

Discussion

We demonstrated that HDGF is mainly expressed in the nucleus of NSCLC cells and that high expression of HDGF

Table II. Multivariate analysis of prognostic factors.

Variables	Unfav./Fav.[a]	Overall survival Risk ratio (95% CI[b])	P-value	Disease-free survival Risk ratio (95% CI)	P-value
Vascular involvement	v (+)/v (-)	1.016 (0.512-2.014)	0.9644	1.044 (0.532-2.048)	0.9009
Smoking	≥40/<40 pack-year	1.398 (0.700-2.792)	0.3427	1.632 (0.815-3.270)	0.1667
pN-factor[c]	N1 + N2/N0	1.462 (0.760-2.811)	0.2548	1.246 (0.649-2.392)	0.5083
Tumor size	>30/≤30 mm	1.572 (0.853-2.895)	0.1468	1.443 (0.782-2.663)	0.2404
Sex	Male/female	1.957 (0.856-4.472)	0.1114	1.956 (0.860-4.450)	0.1096
pStage[c]	III + IV/I + II	1.964 (1.084-3.556)	0.0259	1.848 (1.018-3.355)	0.0436
HDGF	High/low	2.976 (1.641-5.398)	0.0003	2.970 (1.651-5.344)	0.0003

[a]Unfavorable vs. favorable characteristics. [b]CI, confidence interval. [c]According to the AJCC/UICC TNM pathological classification. pStage, pathological stage; pN, pathological lymph node.

is an independent significant factor for worse overall and disease-free survival of patients with completely resected NSCLC. We also showed that HDGF-expression level was associated with both a high Ki-67-LI and a high intratumor MVD.

Recently, Ren *et al* (23) reported that overexpression of HDGF was a marker of poor prognosis only in patients with curatively resected stage I NSCLC. They found no association between HDGF expression and Ki-67-LI of cancer cells, which is inconsistent with our results. This difference may be because our study included stage I-IV cases whereas theirs only included stage I cases: HDGF-expression correlated with Ki-67-LI in stage IB-IV but not in stage IA (data not shown). Thus, we demonstrated that HDGF-expression level is a prognostic factor independent of and more powerful than the pathological stage of NSCLC by the multivariate analysis.

Exogenous HDGF promotes *in vitro* DNA synthesis and cell proliferation in rat and human lung epithelial cells. Endogenous HDGF overexpressed via transient gene transfer was translocated into the nucleus and promoted the proliferation of human lung epithelial A549 cells. Mori *et al* (14) confirmed, using short interfering RNA technique, that endogenously produced HDGF has a mitogenic effect on A549 cells. Collectively, HDGF probably stimulates the proliferation of lung epithelial cells, at least partially, in an autocrine manner. These findings support our result that high expression of HDGF correlates with a high Ki-67-LI of cancer cells. To date it is unknown if the exogenous mitogenic effect of HDGF is mediated by a cell surface receptor or uptake of the protein (4). Further exploration of this mechanism will contribute to the precise understanding of the biological functions of HDGF.

HDGF induced tumorigenesis of NIH3T3 cells in nude mice via direct angiogenic activity and induction of VEGF (7). Moreover, HDGF is a highly expressed vascular endothelial cell protein *in vivo* and is a potent endothelial mitogen and regulator of endothelial cell migration that acts through mechanisms distinct from those of VEGF (6). Since we could not observe a remarkable enhancement of HDGF expression in endothelial cells or vascular smooth muscle cells in NSCLC sections (data not shown), overproduction of HDGF by cancer cells might induce a high intratumor MVD possibly in a paracrine manner.

HDGF shows a homology to high mobility group-1 (HMG-1), a DNA binding protein (24), but lacks the characteristics of an HMG-1 protein, especially of the HMG box responsible for DNA bindings (2). HMG-1 enhances the activity of several transcription factors, including the glucocorticoid receptor, as well as the activity of RAG recombinase (24,25). The molecules controlled by HDGF in the nucleus and subsequent functions of HDGF have not been identified. Therefore, HDGF may display other tumorigenic behavior besides tumor-cell proliferation or angiogenesis.

Bernard *et al* (26) detected HDGF expression mainly in the nucleus and much more strongly in melanoma cell lines than in melanocytes. They showed by immunohistochemical analysis of clinical samples that 54% of benign nevoid cells reacted positively, whereas 78-90% of melanoma cells were positive in all stages of melanoma. We found that HDGF was expressed in ~30-40% of non-cancerous alveolar or bronchial epithelial cells (data not shown) and 20-95% (median 64.5%) of NSCLC cells. The proportion of HDGF-positive cells seems slightly smaller in NSCLC than in melanoma, but our results were in general compatible with those of Bernard *et al* (26). With regard to other malignancies, a recent study using differential display revealed that HDGF expression was associated with radiosensitivity in esophageal cancer (27). Expression profiling of gastric adenocarcinoma using cDNA array revealed that HDGF was one of the overexpressed genes in gastric cancer as compared with normal gastric mucosa (28). Thus, HDGF probably plays a critical role in the development and progression of various malignancies.

Based on the above findings, we consider HDGF is a useful marker of poor prognosis in patients with completely resected NSCLC, and high HDGF-expression might be a potential indicator of the need for adjuvant therapy. Although further investigations need to be done on the molecular characteristics and biological functions of HDGF, this factor may be a target molecule for the treatment of NSCLC.

References

1. Nakamura H, Kambe H, Egawa T, *et al*: Partial purification and characterization of human hepatoma-derived growth factor. Clin Chim Acta 183: 273-284, 1989.

2. Nakamura H, Izumoto Y, Kambe H, *et al*: Molecular cloning of complementary DNA for a novel human hepatoma-derived growth factor. J Biol Chem 269: 25143-25149, 1994.
3. Dietz F, Franken S, Yoshida K, Nakamura H, Kappler J and Gieselmann V: The family of hepatoma-derived growth factor proteins: characterization of a new member HRP-4 and classification of its subfamilies. Biochem J 366: 491-500, 2002.
4. Everett AD and Bushweller J: Hepatoma derived growth factor is a nuclear targeted mitogen. Curr Drug Targets 4: 367-371, 2003.
5. Izumoto Y, Kuroda T, Harada H, Kishimoto T and Nakamura H: Hepatoma-derived growth factor belongs to a gene family in mice showing significant homology in the amino terminus. Biochem Biophys Res Commun 238: 26-32, 1997.
6. Everett AD, Narron JV, Stoops T, Nakamura H and Tucker A: Hepatoma-derived growth factor is a pulmonary endothelial cell-expressed angiogenic factor. Am J Physiol Lung Cell Mol Physiol 286: L1194-L1201, 2004.
7. Okuda Y, Nakamura H, Yoshida K, *et al*: Hepatoma-derived growth factor induces tumorigenesis *in vivo* through both direct angiogenic activity and induction of vascular endothelial growth factor. Cancer Sci 94: 1034-1041, 2003.
8. Oliver JA and Al-Awqati Q: An endothelial growth factor involved in rat renal development. J Clin Invest 102: 1208-1219, 1998.
9. Everett AD, Lobe DR, Matsumura ME, Nakamura H and McNamara CA: Hepatoma-derived growth factor stimulates smooth muscle cell growth and is expressed in vascular development. J Clin Invest 105: 567-575, 2000.
10. Everett AD, Stoops T and McNamara CA: Nuclear targeting is required for hepatoma-derived growth factor-stimulated mitogenesis in vascular smooth muscle cells. J Biol Chem 276: 37564-37568, 2001.
11. Kishima Y, Yamamoto H, Izumoto Y, *et al*: Hepatoma-derived growth factor stimulates cell growth after translocation to the nucleus by nuclear localization signals. J Biol Chem 277: 10315-10322, 2002.
12. Kishima Y, Yoshida K, Enomoto H, *et al*: Antisense oligonucleotides of hepatoma-derived growth factor (HDGF) suppress the proliferation of hepatoma cells. Hepatogastroenterology 49: 1639-1644, 2002.
13. Yoshida K, Nakamura H, Okuda Y, *et al*: Expression of hepatoma-derived growth factor in hepatocarcinogenesis. J Gastroenterol Hepatol 18: 1293-1301, 2003.
14. Mori M, Morishita H, Nakamura H, *et al*: Hepatoma-derived growth factor is involved in lung remodeling by stimulating epithelial growth. Am J Respir Cell Mol Biol 30: 459-469, 2004.
15. Cilley RE, Zgleszewski SE and Chinoy MR: Fetal lung development: airway pressure enhances the expression of developmental genes. J Pediatr Surg 35: 113-119, 2000.
16 Yada I, Wada H and Fujita H: Thoracic and cardiovascular surgery in Japan during 2002: annual report by the Japanese Association for Thoracic Surgery. Jpn J Thorac Cardiovasc Surg 52: 491-508, 2004.
17. The Japan Lung Cancer Society: General rule for clinical and pathological record of lung cancer. (In Japanese). 6th edition. Kanehara Publ. Corp., Tokyo, 2003.
18. Shimizu K, Yoshida J, Nagai K, Nishimura M, Yokose T, Ishii G and Nishiwaki Y: Visceral pleural invasion classification in non-small cell lung cancer: a proposal on the basis of outcome. J Thorac Cardiovasc Surg 127: 1574-1578, 2004.
19. Mountain CF: Revisions in the International System for Staging Lung Cancer. Chest 111: 1710-1717, 1997.
20. Enomoto H, Yoshida K, Kishima Y, *et al*: Hepatoma-derived growth factor is highly expressed in developing liver and promotes fetal hepatocyte proliferation. Hepatology 36: 1519-1527, 2002.
21. Bosari S, Lee AKC, De Lellis RA, Wiley BD, Heatley GJ and Silverman ML: Microvessel quantitation and prognosis in invasive breast carcinoma. Hum Pathol 23: 755-761, 1992.
22. Weidner N: Intratumor microvessel density as a prognostic factor in cancer. Am J Pathol 147: 9-19, 1995.
23. Ren H, Tang X, Lee JJ, *et al*: Expression of hepatoma-derived growth factor is a strong prognostic predictor for patients with early-stage non-small-cell lung cancer. J Clin Oncol 22: 3230-3237, 2004.
24. Bianchi ME and Beltrame M: Upwardly mobile proteins: the role of HMG proteins in chromatin structure, gene expression and neoplasia. EMBO Rep 1: 109-119, 2000.
25. Bustin M: Regulation of DNA-dependent activities by the functional motifs of the high-mobility-group chromosomal proteins. Mol Cel Biol 19: 5237-5246, 1999.
26. Bernard K, Litman E, Fitzpatrick JL, *et al*: Functional proteomic analysis of melanoma progression. Cancer Res 63: 6716-6725, 2003.
27. Matsuyama A, Inoue H, Shibuta K, *et al*: Hepatoma-derived growth factor is associated with reduced sensitivity to irradiation in esophageal cancer. Cancer Res 61: 5714-5717, 2001.
28. El-Rifai W, Frierson HF Jr, Harper JC, Powell SM and Knuutila S: Expression profiling of gastric adenocarcinoma using cDNA array. Int J Cancer 92: 832-838, 2001.